Journal of Photochemistry & Photobiology A: Chemistry 380 (2019) 111843

Contents lists available at ScienceDirect

Journal of Photochemistry & Photobiology A: Chemistry

journal homepage: www.elsevier.com/locate/jphotochem

Photocatalytic activity of rutile/anatase TiO_2 nanorod/nanobranch thin film loaded with Au@Ag@Au core double shell nanoparticles

Shervin Daneshvar e Asl[a,b,*], Sayed Khatiboleslam Sadrnezhaad[a]

[a] Department of Materials Science and Engineering, Sharif University of Technology, Tehran, Iran
[b] Department of Chemistry, National University of Singapore, Singapore

ARTICLE INFO

Keywords:
Rutile/anatase TiO_2
Nanobranched nanorod
Au@Ag@Au core double shell
Photocatalytic activity
Surface plasmon resonance
Energy band engineering

ABSTRACT

A seeding-growth approach was used to prepare Au@Ag@Au core double shell nanoparticles which were loaded on a rutile-nanorods/anatase-nanobranches thin film via the impregnation method. The thin film was synthesized on a fluorine-doped SnO_2 substrate via three stages of (i) $TiCl_4$ treatment, (ii) hydrothermal, and (iii) aqueous chemistry. The photocatalytic capability of the newly developed nanostructure was higher than P25 TiO_2 thin film by 40% under visible light and by 100% under UV light irradiation. Photogenerated charges separation at the junctions of rutile-nanorods and anatase-nanobranches along with localized surface plasmon resonance followed by the hot electron transfer from the core double shell nanoparticles to TiO_2 resulted in the enhancement of photocatalytic activity observed under visible light irradiation. Under UV light illumination, the charge separation effect plus the electron trapping by Au@Ag@Au nanoparticles were responsible for the photocatalytic performance improvement of TiO_2.

1. Introduction

Semiconductor-based photocatalysis has been used widely in the environmental remediation [1]. In this process, the photons excite the valence band electrons of the semiconductor and transfer them to the conduction band. Some positively charged holes would thus remain in the semiconductor's valence band. The resulted electron-hole pairs would lead to the occurrence of the reduction-oxidation reactions on the photocatalyst surface [2–4]. Among many semiconductor materials, titanium dioxide (TiO_2) has received much attention due to its high redox potential, chemical/thermal stability, photo-corrosion resistance, non-toxicity, abundance, and low cost [5–12].

Recombination of the photogenerated charge carriers and the wide band-gap of TiO_2 are the two main limitations of this semiconductors [13,14]. Excited electrons come back to the valence band during recombination processes. It happens in bulk or on the surface of the semiconductors and usually is arisen from defects, impurities, and other surface/bulk imperfections [15–18]. Two common TiO_2 phases, i.e., anatase and rutile, have band-gaps of 3.2 and 3.0 eV, respectively [19]. These values restrict the excitation level to the wavelengths lower than 390 and 413 nm. Consequently, only UV light can activate conventional TiO_2 photocatalyst. Thus, merely about 5% of solar radiations is usable by TiO_2 photocatalysis [20,21]. Approaches like heterojunction formation [22–29], noble metal loading [30–36], ion [37–41] or transition metal [42–47] doping, dye sensitization [48–50], nanosized crystal synthesis, and nonstoichiometric TiO_2 utilization [13,51] are some solutions to resolve these shortcomings.

This paper describes the synthesis procedure and the photocatalytic activity evaluation of the TiO_2 nanobranched nanorods biphasic thin film loaded with bimetallic nanoparticles. The biphasic TiO_2 construction can result in charge separation and efficient transportation [52–54]. The nanobranched nanorods morphology can offer a superior specific surface area and a proper light harvesting network [54,55]. Noble metal nanoparticles can absorb visible light and scatter photon, based on localized surface plasmon resonance (LSPR) characteristic [56]. LSPR refers to the collective oscillations of metal particle electrons by the electromagnetic field induced by incident light [57]. Among different metallic nanoparticles, silver is the most efficient one in increasing TiO_2 photocatalytic activity via visible light absorption based on LSPR [58,59]. However, silver nanoparticles' exposure to oxidation leads to silver oxide formation in the interface of silver and TiO_2 [60] which shifts LSPR wavelength and declines the photoabsorption intensity [61,62]. Moreover, the preparation of uniform silver nanoparticles in the solution is too complicated [63]. So, Au@Ag@Au core double shell nanostructure is a desirable structure. Owing to the excitation of the silver layer LSPR, the new structure leads to efficient visible light absorption and electron transfer towards the semiconductor layer. Meanwhile, the presence of the gold shell

* Corresponding author at: Department of Materials Science and Engineering, Sharif University of Technology, Tehran, Iran.
E-mail addresses: sh.dan4@student.sharif.edu, CHMV171@nus.edu.sg (S. Daneshvar e Asl), sadrnezh@sharif.edu (S.K. Sadrnezhaad).

https://doi.org/10.1016/j.jphotochem.2019.05.006
Received 17 February 2019; Received in revised form 23 April 2019; Accepted 2 May 2019
Available online 11 May 2019
1010-6030/ © 2019 Elsevier B.V. All rights reserved.

Nomenclature

A*	Constant (unitless)	h	Planck's constant (4.135×10^{-15} eV.s)
c_0	Dye concentration after absorption in darkness (M)	k	Rate constant of reaction (min^{-1})
c	Dye concentration after irradiation for a duration of $t > 0$ (M)	m	Constant, = 2 for indirect allowed transition
d	Thin film thickness (cm)	t	Irradiation time (min)
E_g	Optical indirect band-gap (eV)	T	Thin film transmittance (%)
		α	Thin film absorption coefficient (cm^{-1})
		υ	Frequency (s^{-1})

prevents silver oxidation and causes stabilization of the LSPR under irradiation and gold core facilitates the preparation of the nanoparticles with controllable size. Furthermore, as the d-band center of the bimetallic nanoparticles can be close to the Fermi level, these nanoparticles tend to display high activity in the reduction reaction of oxygen molecules, which causes to form more superoxide radicals, leading to enhance the photocatalytic performance [64].

2. Materials and methods

2.1. Materials

Fluorine-doped tin oxide (FTO) glass was purchased from Zhuhai Kaivo Electronic Components Co., Ltd. Titanium(IV) butoxide, gold(III) chloride, sodium borohydride, and cetyltrimethylammonium chloride solution (CTAC, 25 wt.% in H_2O) were bought from Aldrich. Titanium tetrachloride, ammonium hexafluorotitanate, and silver nitrate were purchased from Sigma-Aldrich. 2-propanol and acetone were bought from AnalaR NORMAPUR®. Tri-sodium citrate dihydrate, L-ascorbic acid, sodium chloride, hydrochloric acid (37 wt.%), boric acid, and Rhodamine B were purchased from Fluka, Sigma Life Science, Uni-Chem, Schedelco, Merck, and Lancaster, respectively. All reagents were of analytical grade and used as received. The grade of water used in different stages was deionized (DI) water.

2.2. Synthesis

Rutile/anatase TiO_2 nanorod/nanobranch thin film on the FTO substrate was synthesized via a multi-step growth process according to our previous work [65], as shown in Scheme 1. Hereafter, thin films of nanorods and nanobranched nanorods are abbreviated as NRs and NBNRs, respectively.

Au@Ag@Au core double shell nanoparticles were synthesized via a multi-step growth process. In detail, spherical gold nanoparticles were synthesized via a two-step process modified from previously reported methods [66–70]. At first, a solution including gold seeds was prepared. For this purpose, 10 ml of growth solution containing gold precursor (0.25 mM) and trisodium citrate dehydrate (0.25 mM) was made. Then, 300 µl of 100 mM sodium borohydride solution (reducing agent) was added to the growth solution immediately after preparation, while vigorously shaking by a magnetic stirrer which continued for 2 min. It is of great importance to let the produced gases during the reaction escape. Upon addition of sodium borohydride and gold seeds formation, the color of the solution would be orange-red. After that, the solution of gold seeds was kept at room temperature for four hours to decompose the excess borohydride. It is worth noting that ice-cold DI water was used for the preparation of the sodium borohydride solution. In related trisodium citrate, citrate acts as the capping agent and prevents seeds hyper-growth and their various sizes. It is necessary to mention that citrate cannot reduce gold salt at room temperature. On the other hand, citrate stabilizes seeds in the solution by generating negative charges on them. After that, the seed solution was utilized for gold nanoparticles synthesis. For this purpose, 1.125 ml of 10 mM gold precursor solution was added to 45 ml of 80 mM CTAC solution (as nanoparticles stabilizer), while stirring with a magnetic stirrer. The color of the solution would be yellowish by the introduction of the gold precursor and its dissolution. Then, 250 µl of freshly prepared 100 mM ascorbic acid solution (reducing agent), was added to the previous solution while stirring. In this step, the solution would be transparent and colorless due to Au^{3+} ions reduction to Au^{+}. Eventually, 2.5 ml of the seed solution was added to this solution. In this stage, Au^{+} ions were reduced to Au^{0}, and the color of the solution would be ruby red that indicates gold nanoparticles formation. Solution stirring was continued for 10 min until the complete reduction of the gold salt. The solution of gold nanoparticles was kept at room temperature for three hours before further usage. CTAC-covered gold nanoparticles were positively charged. It should be noticed that if the solution of gold seeds was added before the ascorbic acid solution, the rate of reaction would be too slow.

Spherical Au@Ag core shell nanoparticles were prepared by using a procedure similar to a protocol that was previously used for the preparation of Au@Ag nanorods [66]. For this purpose, 10 ml of the solution including Au nanoparticles was first centrifuged with a speed of 14,000 rpm for 45 min and then washed with 0.08 M CTAC solution two times at the similar centrifuging conditions and finally re-dispersed into the same volume of CTAC solution. Then, 300 µl of freshly prepared 100 mM ascorbic acid solution (reducing agent) and 200 µl of 10 mM silver precursor solution were added to this solution, respectively while stirring with a magnetic stirrer. Afterward, the solution was stirred in a 60 °C water bath for one hour. During this step, the color of the solution was changed from ruby red to orange, which shows silver shell formation on the gold nanoparticles surfaces. The solution of Au@Ag nanoparticles was kept at room temperature for three hours before the next usage. Au@Ag@Au core double shell nanoparticles were prepared using 10 ml of the solution including Au@Ag nanoparticles, as the seed solution, via the same method as gold nanoparticles synthesis. The color of the final solution would be purple which indicates Au@Ag@Au nanoparticles formation.

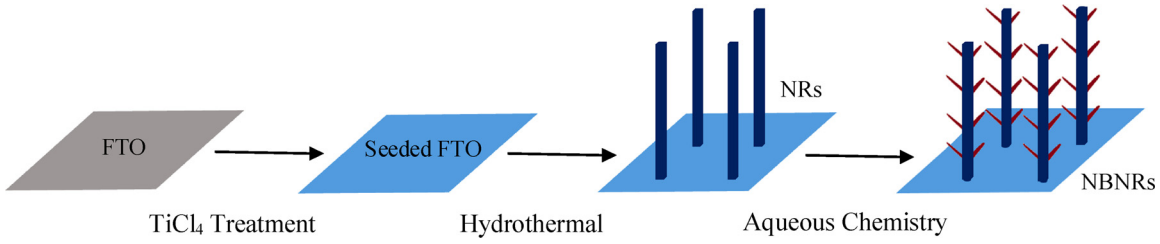

Scheme 1. Synthesis steps of rutile/anatase TiO_2 nanorod/nanobranch thin film.

Au@Ag@Au nanoparticles were loaded on TiO_2 NBNRs thin film via an impregnation method. NBNRs thin film put into the solution of core double shell nanoparticles and solvent dried by using an evaporator on a water bath. Before impregnation, the nanoparticles centrifuged with a speed of 14,000 rpm for 45 min and re-dispersed in DI water. Hereafter, TiO_2 NBNRs thin film loaded with Au@Ag@Au nanoparticles is abbreviated as NBNRs-Au@Ag@Au.

2.3. Photocatalytic activity tests

The photocatalytic performances of thin films of TiO_2 NRs, NBNRs, and NBNRs-Au@Ag@Au were determined by photocatalytic decomposition of Rhodamine B (Rh B) dye (Supplementary Figure S1). For comparison, a thin film of P25 TiO_2 nanoparticles was also synthesized [71] and used as the benchmark. For photocatalytic tests, TiO_2 thin films (2.5 × 2.5 cm × cm in size) were put in 60 cc of 5 μM Rh B solution in a water jacketed reactor under UV and visible irradiation, as shown in Supplementary Schematic S1. Before irradiation, the reactor was kept in darkness overnight in order to achieve the equilibrium absorption level. The solution was exposed to air during the test and stirred by a magnetic stirrer. The distance between the light source and the surface of the solution was 10 cm, and the density power of UV and visible light were about 5 and 200 mW/cm^2, respectively. The solution was irradiated for 90 min, and its concentration was evaluated at 15-minute intervals. Each photocatalytic test was repeated three times, and the average values were used in drawing curves.

Photodegradation curves can be fitted with pseudo-first-order kinetic [72]:

$$\mathrm{Ln}\ (c_0/c) = kt \quad (1)$$

In Eq. (1), c_0 is the dye concentration after absorption in darkness, c is its concentration after irradiation for a duration of $t > 0$, and k is the rate constant of the reaction.

2.4. Instrumentations and characterizations

Micrographs images of field emission scanning electron microscope (FESEM) and transmission electron microscope (TEM) were taken on JEOL JSM-6701 F and JEOL JEM-3011 microscopes, respectively. To prepare the sample of the core double shell nanoparticles for TEM characterization, one drop of the five-fold concentrated solution poured on a copper grid. Energy dispersive spectra (EDS) were examined with JEOL JED-2300 installed to the FESEM. The XRD patterns were recorded in an X'Pert PRO MPD (PANalytical) with Cu Kα radiation (λ = 0.15406 nm). The X-ray tube voltage and current were set at 40 kV and 40 mA, respectively. The Raman spectra were collected using a Horiba Jobin Yvon modular Raman spectrometer equipped with a Stellar Pro Argon-ion laser operating at 514 nm with an incident power of 50 mW. The photoluminescence (PL) emission spectra were determined on a Horiba Jobin Yvon fluoromax-4 spectrofluorometer with an exciting wavelength of 350 nm. The diffuse transmittance spectra (DTS) were measured using a UV–Vis spectrophotometer (Avaspec-2048-TECwith AvaLamp DH-S Setup) with an integrating sphere attachment. For determining the concentration changes of the Rh B solution by passing the time, its absorption spectra were recorded by using a Hitachi UH5300 double beam spectrophotometer at the wavelength of 554 nm. This instrument was also used for the recording of core double shell nanoparticles extinction spectra. PLS-SXE300UV300 was utilized as the light source in combination with suitable optical filters in photocatalytic tests. In detail, the irradiation was provided by a 50 W xenon light source and a 420 nm UV-cut filter was used in visible light photocatalytic tests.

3. Results and discussion

The morphologies of TiO_2 thin films were examined with FESEM. Fig. 1 indicates FESEM images of TiO_2 NRs and NBNRs thin films. Fig. 1(a) shows that the coating consisting of nanorods is uniform and they have vertical growth direction, an average diameter of 90 ± 1 nm, estimated density of 5*10^9 NRs/cm^2 and height of 3.6 μm. As it is evident from images, nanorods are tetragonal with a square upper surface (the expected way for tetragonal growth). As it is observed in Fig. 1(b), nanobranches have grown monotonously on the surface of nanorods. As a result, surface area and light harvesting capability of the coating enhances significantly. This increase would benefit to TiO_2 photoelectrochemical activity improvement [73].

Fig. 2 shows a TEM photograph and extinction spectrum of colloidal Au@Ag@Au nanoparticles. As it is observed in Fig. 2(a), core double shell nanoparticles are polyhedral with the mean particle size of 31 ± 1 nm. The photograph shows a homogeneous distribution of nanoparticles. As it is seen in Fig. 2(b), the nanoparticles show a plasmon absorption in the visible range at 542 nm. The narrow peak indicates nanoparticles no-congregation. Since Au is biocompatible and stable, and Ag is a highly sensitive element, Au@Ag@Au nanoparticles are highly sensitive, stable and biocompatible.

The chemical stoichiometry of the thin films was examined with EDS. Fig. 3 indicates energy diffraction spectra and elemental compositions of TiO_2 NRs and NBNRs thin films. As it is observed, the atomic

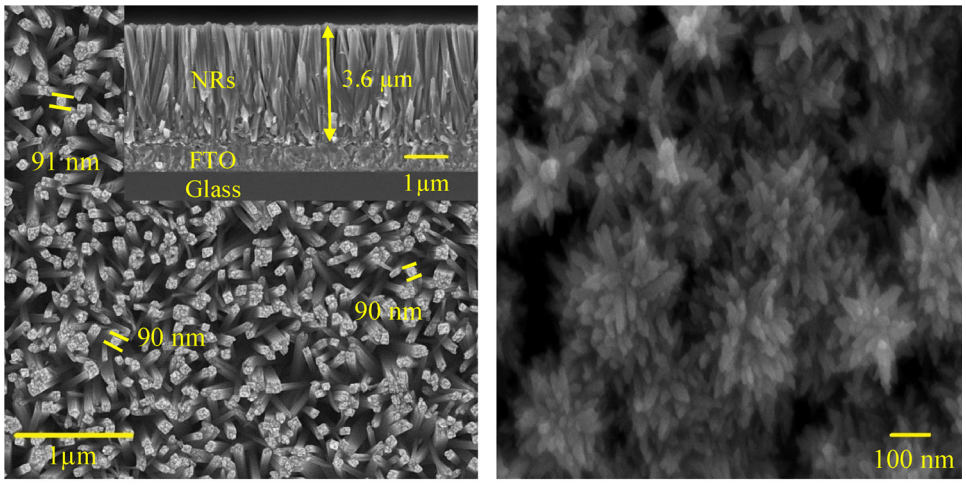

(a) (b)

Fig. 1. FESEM images of TiO_2 (a) NRs and (b) NBNRs thin films. The inset of (a) shows an image of the cross-sectional view of NRs.

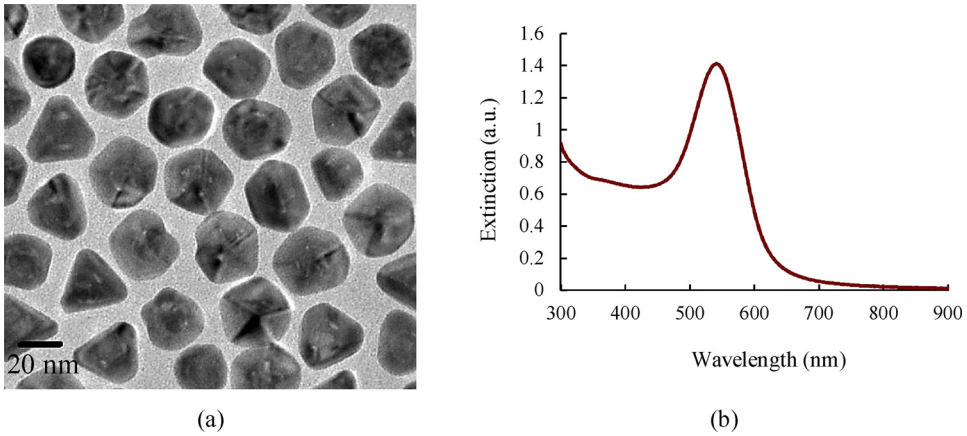

Fig. 2. TEM photograph (a) and extinction spectrum (b) of colloidal Au@Ag@Au nanoparticles.

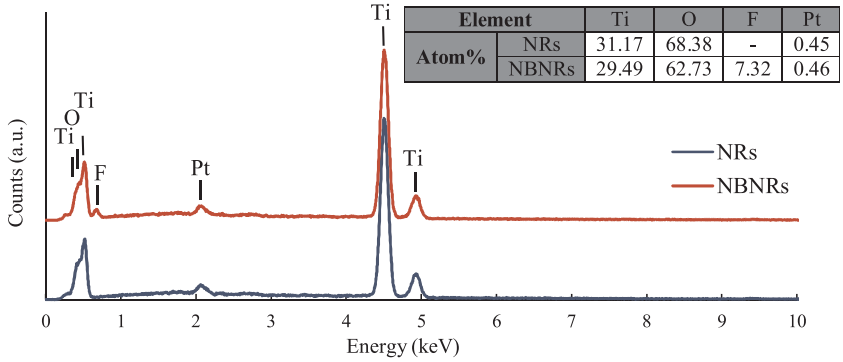

Element		Ti	O	F	Pt
Atom%	NRs	31.17	68.38	-	0.45
	NBNRs	29.49	62.73	7.32	0.46

Fig. 3. Energy diffraction spectra and elemental compositions of TiO_2 NRs and NBNRs thin films.

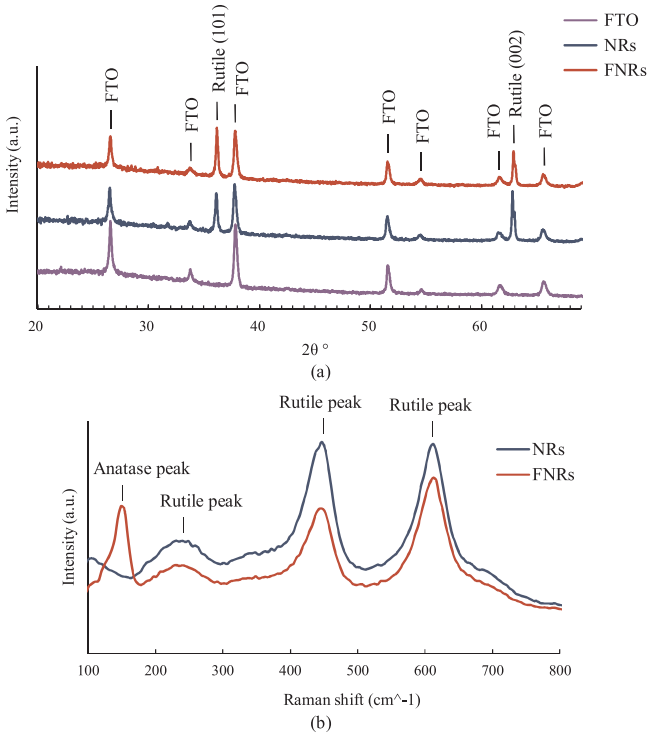

Fig. 4. (a) XRD of the FTO substrate and TiO_2 NRs and NBNRs thin films and (b) Raman spectrums of TiO_2 thin films.

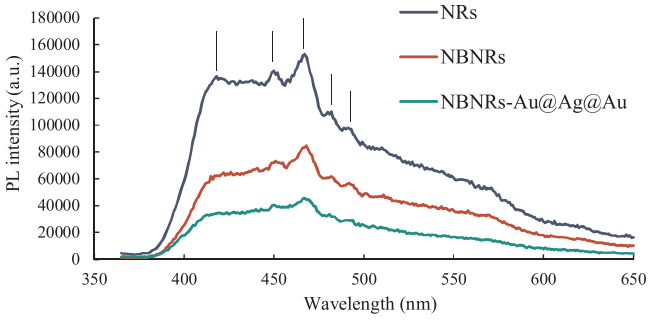

Fig. 5. PL emission spectra of TiO_2 NRs, NBNRs, and NBNRs-Au@Ag@Au thin films.

rate of Ti to O in the thin films is slightly less than 0.5, which means excess oxygen in the semiconductor, probably due to the adsorption of oxygen on the surface of the thin film. The NBNRs spectrum displays F signal that is probably due to its doping in the structure by replacement with O^{2-} ions during synthesis from titanium precursor. Pt has covered thin films in coating step to make them ready for electron microscopy.

The crystal structure and crystalline phase of TiO_2 thin films were evaluated with XRD and Raman spectroscopy. XRD spectrums of FTO substrate, TiO_2 NRs and NBNRs thin films are indicated in Fig. 4(a), which makes it clear that the coated film on FTO is TiO_2. Arisen diffraction peaks are attributed to rutile with tetragonal crystalline structure (a = b = 0.459 nm, c = 0.295 nm [19]). The diffraction peak (002) has improved considerably, and some of the diffraction peaks have been removed, in comparison with powder diffraction pattern, implying that synthesized nanorods have oriented and grown perpendicular to the substrate surface in [001] direction. The lattice mismatch between FTO (tetragonal, a = b = 0.4687 nm [74]) and rutile TiO_2 on

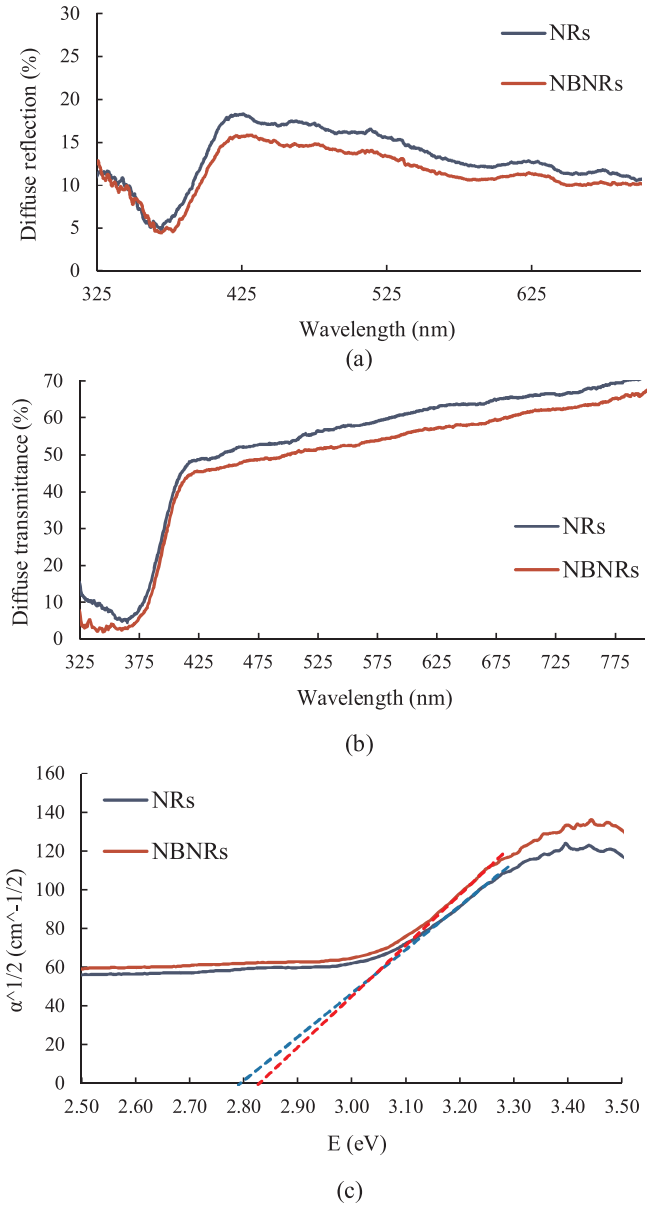

Fig. 6. (a) Diffused reflectance and (b) diffuse transmittance spectra, and (c) band-gap energy estimation of TiO_2 NRs and NBNRs thin films.

(001) plane, is only 2%. Therefore, nanorods epitaxial nucleation and their growth direction have been improved by expanding (001) plane at the interface in the seed layer precipitation step. Raman spectroscopy was also utilized to obtain a more scrupulous characterization. Fig. 4(b) illustrates the Raman spectrums of TiO_2 NRs and NBNRs thin films. Three peaks appear in 245 cm^{-1}, 442 cm^{-1} and 609 cm^{-1} for TiO_2 nanorods that are rutile characteristic peaks, and a peak arises in 161 cm^{-1} for TiO_2 NBNRs, in addition to those previous peaks, which is anatase characteristic (tetragonal, a = b = 0.378 nm, c = 0.950 nm [19]). So, it is conspicuous that anatase nanobranches have been formed on rutile nanorods. Thus, the anatase phase has been formed while low-temperature synthesis and without annealing, and it can be a benefit because annealing temperature may result in nanostructure agglomeration, deformation, and specific surface area decrease. Anatase phase peaks have not appeared in the XRD spectrum of the NBNRs due to the partial amount of nanobranches in comparison with nanorods. Photogenerated electron-hole pairs in rutile nanorods can separate from each other via electron transfer to anatase nanobranches [75]. Separation of charge carriers and having greater lifetime improve TiO_2 photoelectrochemical activity [76].

The photoluminescence emission spectrum was utilized for examination the efficiency of trapping, immigration, transfer, and separation of charge carriers and understanding the lifetime of photogenerated electron-hole pairs in TiO_2, because P1 emission results from free charge carriers recombination [77–79]. Fig. 5 shows photoluminescence spectrums of TiO_2 NRs, NBNRs, and NBNRs-Au@Ag@Au thin films. Emission peak in 420 nm is attributed to direct band transition with the energy of light approximately equal to the band-gap energy, and emission peaks in 451 and 468 nm are ascribed to band edge free excitons. Two emission peaks around 490 nm are accredited to excitonic Pl which are caused by surface oxygen vacancies or defects [80]. As it is observed, P1 signals intensity in NBNRs is weaker than NRs, that demonstrates NBNRs have lower electron-holes recombination rate. The reason is charge carriers separation due to electron transfer from rutile nanorods to anatase nanobranches. The NBNRs-Au@Ag@Au exhibit the lowest recombination rate due to further separation of charge carriers as a result of electron transfer from TiO_2 to the core double shell nanoparticles.

To study the optical properties of TiO_2 thin films UV–vis spectra were utilized. Diffused reflectance and diffuse transmittance spectra of TiO_2 NRs and NBNRs thin films are shown in Fig. 6(a) and (b). TiO_2 NBNRs have a better light harvesting capability owing to their particular morphology, as it is obvious from curves. That is to say, this thin film scatters radiated light superiorly and offers better motion pathways; as a result, radiated photons-TiO_2 interaction increase causes higher photoelectrochemical efficiency [81]. Light absorption proportional to TiO_2 band-gap, leads to curves abrupt drop in wavelengths of around 420 nm.

Band-gap energy of TiO_2 thin films was measured by optical transmittance method [82–85]. Absorption coefficient near the absorption edge is determined by Eq. (2):

$$\alpha = -(1/d)\,\mathrm{Ln}\,(T) \tag{2}$$

Eq. (3) designates absorption coefficient dependence on radiated light energy, above the absorption threshold:

$$\alpha \cong A^{*}(h\upsilon - E_g)^{m} \tag{3}$$

Where α is the absorption coefficient (gained from light transmission and film thickness), d is film thickness (cm), T is transmittance (%), A^* is a constant that does not depend on hυ (unitless), υ is frequency (s^{-1}), h is Planck's constant (4.135×10^{-15} eV.s), and E_g is the indirect optical band-gap (eV), which is indirect in the case of anatase and rutile [76,82,84–86].

$\alpha^{1/2}$ (m = 2 for indirect allowed transition [76]) is traced on the ordinate against photon energy (hυ) on the abscissa, to estimate band-gap energy. The intercept of the tangent to the absorption edge with the abscissa is an approximation of band-gap energy.

Fig. 6(c) indicates the band-gap energy estimation of TiO_2 thin films. As it is conspicuous, the values of band-gap energy for NRs and NBNRs are 2.80 eV and 2.84 eV, respectively. The significant oxygen deficiency arising from the low-temperature synthesis route causes synthesized thin film to have a lower band-gap, in comparison with typical values of TiO_2. Band-gap increase of NBNRs in comparison with NRs is due to the partial existence of anatase nanobranches besides rutile nanorods.

Rh B photodegradation curves in the absence and presence of different TiO_2 thin films under UV and Vis light irradiation and fitting results assuming a pseudo-first order reaction are shown in Fig. 7.

The mechanism of photocatalytic degradation of Rh B by NRs, NBRDs, and NBRDs-Au@Ag@Au under visible and UV light irradiation is illustrated in Scheme 2. It has been proven that the rutile and anatase phase junction prevents photogenerated electron-hole pairs from recombination, but charge transfer direction between two phases is still ambiguous. In the schematic, the energetic alignment of the band edges

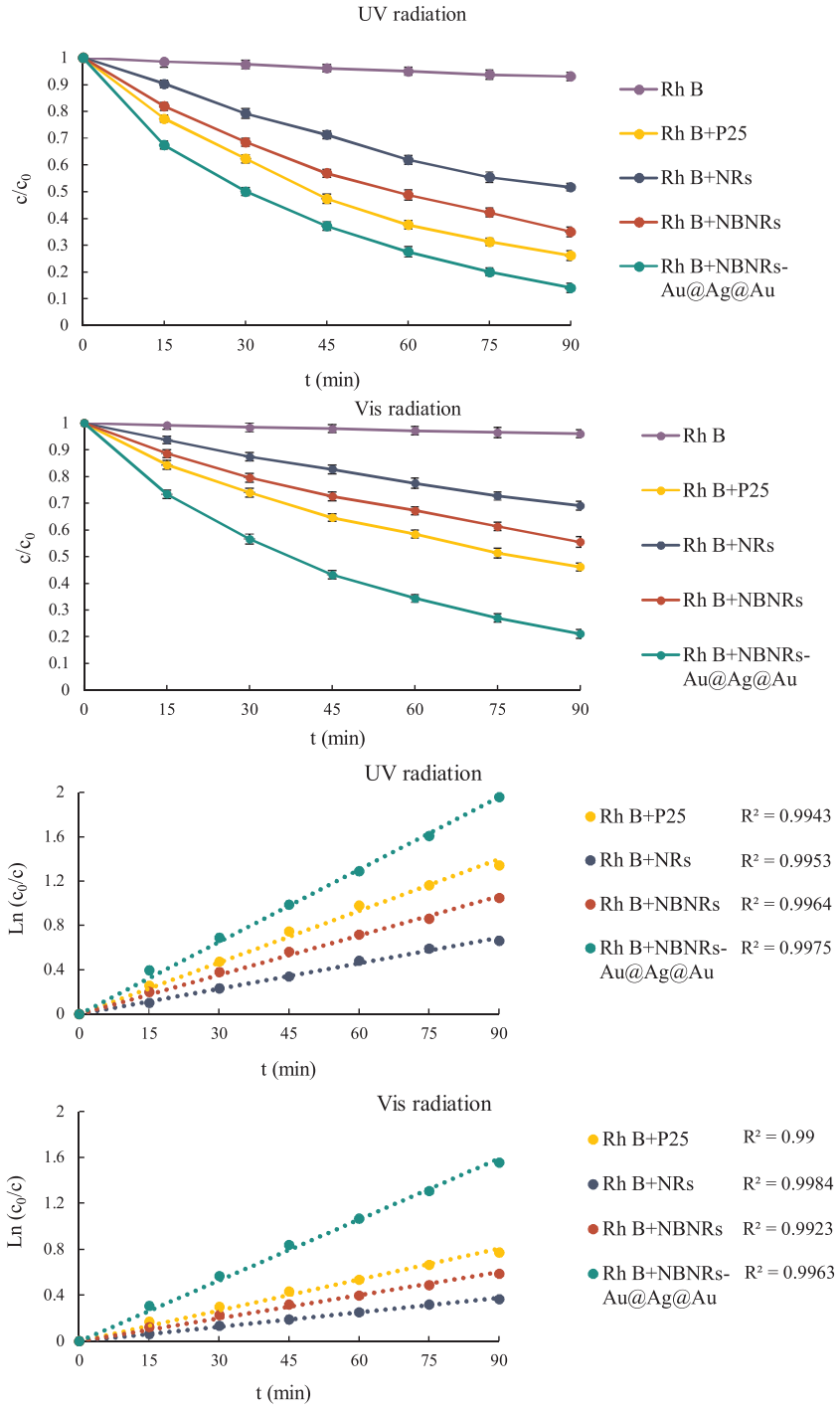

Fig. 7. Rh B photodegradation curves in the absence and presence of different TiO_2 thin films under UV and Vis light irradiation and fitting results assuming a pseudo-first order reaction.

of rutile and anatase, which has been suggested by Scanlon et al. [75], is used. Also, given that superoxide radicals (O_2^-) are the major active species responsible for photocatalytic oxidation reaction [53], the photodegradation route via e^- and O_2^- is shown in the schematic. Considering that band-gap energy values for synthesized NRs and NBNRs thin films are 2.80 and 2.84 eV, respectively (Fig. 6 (c)), which are proportional to wavelengths of 443 and 436 nm, photon absorption is considered to be done by rutile nanorods and photocatalytic reaction would be performed under visible light ($\lambda < 420$ nm) (as photocatalytic tests results confirm it). Furthermore, after nanorods being nanobranched, the photocatalytic reaction continues on the surface of nanobranches, because nanobranches cover nanorods completely (Fig. 1 (b)).

As it is indicated in Supplementary Table S1, absorption capacity in darkness in NBNRs and NBNRs-Au@Ag@Au is increased due to higher specific surface area and nanoparticles-dye molecules interaction. In the absence of photocatalyst, 4 and 7% of dye molecules are decomposed during 90 min under visible and UV light irradiation, respectively.

The reason for photocatalytic activity enhancement in NBNRs in comparison with NRs is that the former has a biphasic structure and charge separation is improved by electron transfer from rutile to

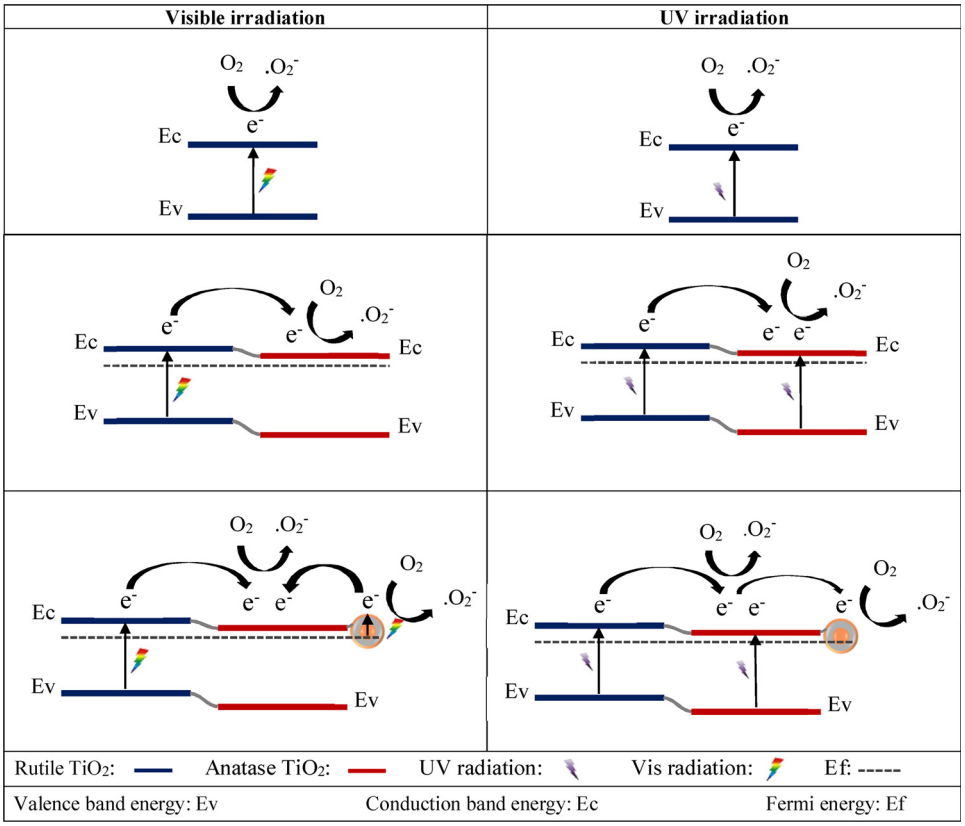

Scheme 2. The schematic mechanism of the photocatalytic degradation of RB by TiO_2 NRs, NBRDs, and NBRDs-Au@Ag@Au under the visible and UV irradiation.

Table 1
The rate constants of the reaction (k, min^{-1}) of different TiO_2 thin films under visible and UV irradiation.

TiO_2 thin films	Rutile\Anatase P25 NPs	Rutile NRs	Rutile\Anatase NBNRs	Rutile\Anatase NBNRs-Au@Ag@Au
Rh B + Vis	$1.55*10^{-2}$	$0.76*10^{-2}$	$1.18*10^{-2}$	$2.18*10^{-2}$
Rh B + UV	$0.90*10^{-2}$	$0.42*10^{-2}$	$0.67*10^{-2}$	$1.77*10^{-2}$

anatase. Moreover, it has been determined that oxygen reduction is not sufficient by the photogenerated electrons on the surface of rutile, because of low tendency between surface and oxygen and anatase is more active in oxygen reduction [87]. It should be noted that NBNRs have a higher surface area and light harvesting capability (Fig. 6(a) and (b)).

Core double shell nanoparticles loading enhances the photocatalytic activity of TiO_2 NBNRs thin film under both visible and UV light irradiation, because of LSPR characteristic and electron trapping, respectively. Under UV light radiation, Schottky barrier between core double shell nanoparticle and TiO_2 causes photogenerated electrons transfer from TiO_2 to the metal, and this leads to more separation of charge carriers and as a result, more increase in photocatalytic activity in comparison with NBNRs without nanoparticles. Under visible light radiation, core double shell nanoparticle can inject the electrons into TiO_2 via LSPR characteristic and improve its photocatalytic activity. TiO_2 NBNR-Au@Ag@Au represents enhanced photocatalytic performance in comparison with P25 TiO_2 under both visible and UV light irradiation. The rate constants of the reaction of different TiO_2 thin films under visible and UV light irradiation are summarized in Table 1.

4. Conclusions

Rutile/anatase TiO_2 nanorod/nanobranch thin film loaded with Au@Ag@Au core double shell nanoparticles was successfully synthesized, and its photocatalytic performance in the dye photodegradation under visible and UV light irradiation was measured and discussed. The improved photocatalytic activity of TiO_2 under light illumination was ascribed to the photogenerated charges separation at the interface of rutile-nanorod/anatase-nanobranch junctions, electron trapping by loaded nanoparticles (under UV light irradiation), and hot electron injection from the core double shell nanoparticles to TiO_2 based on localized surface plasmon resonance characteristic of the metallic nanoparticles (under visible light irradiation).

Data availability

The raw/processed data required to reproduce these findings cannot be shared at this time as the data also forms part of an ongoing study.

Acknowledgments

Professor Q.H. Xu at NUS is appreciated for providing synthesis and characterization facilities. This work was supported by Iran Nanotechnology Initiative Council, Iran's National Elites Foundation, and Iran National Science Foundation.

Appendix A. Supplementary data

Supplementary material related to this article can be found, in the online version, at doi:https://doi.org/10.1016/j.jphotochem.2019.05.006.

References

[1] B. Ohtani, Preparing articles on photocatalysis— beyond the illusions, misconceptions, and speculation, Chem. Lett. 37 (2008) 217–229.
[2] R. Pawar, C.S. Lee, Basics of photocatalysis, Heterog. Nanocomposite-Photocatalysis

Water Purif. 1st ed., Elsevier, United States, 2015, pp. 1–23.
[3] R. Leary, A. Westwood, Carbonaceous nanomaterials for the enhancement of TiO_2 photocatalysis, Carbon 49 (2011) 741–772.
[4] R. Fagan, D.E. McCormack, D.D. Dionysiou, S.C. Pillai, A review of solar and visible light active TiO_2 photocatalysis for treating bacteria, cyanotoxins and contaminants of emerging concern, Mater. Sci. Semicond. Process. 42 (2016) 2–14.
[5] M.R. Hoffmann, S.T. Martin, W. Choi, D.W. Bahnemannt, Environmental applications of semiconductor photocatalysis, Chem. Rev. 95 (1995) 69–96.
[6] D. Shi, Z. Guo, N. Bedford, Nanotitanium oxide as a photocatalytic material and its application, Nanomater. Devices, 1st ed., Elsevier, United States, 2015, pp. 161–174.
[7] Y. Wang, Y. Huang, W. Ho, L. Zhang, Z. Zou, S. Lee, Biomolecule-controlled hydrothermal synthesis of C–N–S-tridoped TiO_2 nanocrystalline photocatalysts for NO removal under simulated solar light irradiation, J. Hazard. Mater. 169 (2009) 77–87.
[8] C. Su, C.-M. Tseng, L.-F. Chen, B.-H. You, B.-C. Hsu, S.-S. Chen, Sol–hydrothermal preparation and photocatalysis of titanium dioxide, Thin Solid Films 498 (2006) 259–265.
[9] M. Pelaez, P. Falaras, V. Likodimos, A.G. Kontos, A.A. de la Cruz, K. O'Shea, D.D. Dionysiou, Synthesis, structural characterization and evaluation of sol–gel-based NF-TiO_2 films with visible light-photoactivation for the removal of microcystin-LR, Appl. Catal. B Environ. Environ. 99 (2010) 378–387.
[10] P. Swarnakar, S.R. Kanel, D. Nepal, Y. Jiang, H. Jia, L. Kerr, M.N. Goltz, J. Levy, J. Rakovan, Silver deposited titanium dioxide thin film for photocatalysis of organic compounds using natural light, Sol. Energy 88 (2013) 242–249.
[11] C. Comninellis, A. Kapalka, S. Malato, S.A. Parsons, I. Poulios, D. Mantzavinos, Advanced oxidation processes for water treatment: advances and trends for R&D, J. Chem. Technol. Biotechnol. 83 (2008) 769–776.
[12] J.M. Poyatos, M.M. Muñio, M.C. Almecija, J.C. Torres, E. Hontoria, F. Osorio, Advanced oxidation processes for wastewater treatment: state of the art, Water Air Soil Pollut. 205 (2010) 187–204.
[13] V. Etacheri, M.K. Seery, S.J. Hinder, S.C. Pillai, Oxygen rich titania: a dopant free, high temperature stable and visible-light active anatase photocatalyst, Adv. Funct. Mater. 21 (2011) 3744–3752.
[14] W. Choi, A. Termin, M.R. Hoffmann, The role of metal ion dopants in quantum-sized TiO_2: correlation between photoreactivity and charge carrier recombination dynamics, J. Phys. Chem. 98 (1994) 13669–13679.
[15] X. Chen, S.S. Mao, Titanium dioxide nanomaterials: synthesis, properties, modifications, and applications, Chem. Rev. 107 (2007) 2891–2959.
[16] A. Sclafani, J.M. Herrmann, Comparison of the photoelectronic and photocatalytic activities of various anatase and rutile forms of titania in pure liquid organic phases and in aqueous solutions, J. Phys. Chem. 100 (1996) 13655–13661.
[17] J. Liqiang, Q. Yichun, W. Baiqi, L. Shudan, J. Baojiang, Y. Libin, F. Wei, F. Honggang, S. Jiazhong, Review of photoluminescence performance of nano-sized semiconductor materials and its relationships with photocatalytic activity, Sol. Energy Mater. Sol. Cells 90 (2006) 1773–1787.
[18] N. Serpone, Relative photonic efficiencies and quantum yields in heterogeneous photocatalysis, J. Photochem. Photobiol. A: Chem. 104 (1997) 1–12.
[19] V. Etacheri, C. Di Valentin, J. Schneider, D. Bahnemann, S.C. Pillai, Visible-light activation of TiO_2photocatalysts: advances in theory and experiments, J. Photochem. Photobiol. C Photochem. Rev. 25 (2015) 1–29.
[20] V. Etacheri, M.K. Seery, S.J. Hinder, S.C. Pillai, Nanostructured $Ti_{1-x}S_xO_{2-y}N_y$ heterojunctions for efficient visible-light-induced photocatalysis, Inorg. Chem. 51 (2012) 7164–7173.
[21] Y.Q. Wang, X.J. Yu, D.Z. Sun, Synthesis, characterization, and photocatalytic activity of $TiO_{2-x}N_x$ nanocatalyst, J. Hazard. Mater. 144 (2007) 328–333.
[22] S. Feizpoor, A. Habibi-Yangjeh, S. Vadivel, Novel TiO_2/Ag_2CrO_4nanocomposites: efficient visible-light-driven photocatalysts with n-n heterojunctions, J. Photochem. Photobiol. A: Chem. 341 (2017) 57–68.
[23] X. Li, X. Chen, H. Niu, X. Han, T. Zhang, J. Liu, H. Lin, F. Qu, The synthesis of CdS/TiO_2 hetero-nanofibers with enhanced visible photocatalytic activity, J. Colloid Interface Sci. 452 (2015) 89–97.
[24] I. Tamiolakis, I.N. Lykakis, G.S. Armatas, Mesoporous CdS-sensitized TiO_2 nanoparticle assemblies with enhanced photocatalytic properties: selective aerobic oxidation of benzyl alcohols, Catal. Today 250 (2015) 180–186.
[25] R. Hao, G. Wang, C. Jiang, H. Tang, Q. Xu, In situ hydrothermal synthesis of g-C_3N_4/TiO_2 heterojunction photocatalysts with high specific surface area for Rhodamine B degradation, Appl. Surf. Sci. 411 (2017) 400–410.
[26] J. Li, M. Zhang, X. Li, Q. Li, J. Yang, Effect of the calcination temperature on the visible light photocatalytic activity of direct contact Z-scheme g-C_3N_4-TiO_2 heterojunction, Appl. Catal. B Environ. 212 (2017) 106–114.
[27] Y. Cao, Z. Xing, Z. Li, X. Wu, M. Hu, X. Yan, Q. Zhu, S. Yang, W. Zhou, Mesoporous black TiO_{2-x}/Ag nanospheres coupled with g-C_3N_4 nanosheets as 3D/2D ternary heterojunctions visible light photocatalysts, J. Hazard. Mater. 343 (2018) 181–190.
[28] B. Choi, J. Song, M. Song, B.S. Goo, Y.W. Lee, Y. Kim, H. Yang, S.W. Han, Core-shell engineering of Pd-Ag bimetallic catalysts for efficient hydrogen production from formic acid decomposition, ACS Catal. 9 (2019) 819–826.
[29] Y.-L. Liu, J.M. Wu, Synergistically catalytic activities of $BiFeO_3/TiO_2$ core-shell nanocomposites for degradation of organic dye molecule through piezophototronic effect, Nano Energy 56 (2019) 74–81.
[30] M. Li, Z. Yu, Q. Liu, L. Sun, W. Huang, Photocatalytic decomposition of perfluorooctanoic acid by noble metallic nanoparticles modified TiO_2, Chem. Eng. J. 286 (2016) 232–238.
[31] Q. Zhang, R. Li, Z. Li, A. Li, S. Wang, Z. Liang, S. Liao, C. Li, The dependence of photocatalytic activity on the selective and nonselective deposition of noble metal cocatalysts on the facets of rutile TiO_2, J. Catal. 337 (2016) 36–44.
[32] S. Sakthivel, M. Shankar, M. Palanichamy, B. Arabindoo, D. Bahnemann, V. Murugesan, Enhancement of photocatalytic activity by metal deposition: characterisation and photonic efficiency of Pt, Au and Pd deposited on TiO_2 catalyst, Water Res. 38 (2004) 3001–3008.
[33] L.G. Devi, R. Kavitha, A review on plasmonic metal-TiO_2 composite for generation, trapping, storing and dynamic vectorial transfer of photogenerated electrons across the Schottky junction in a photocatalytic system, Appl. Surf. Sci. 360 (2016) 601–622.
[34] N.S. Kolobov, D.A. Svintsitskiy, E.A. Kozlova, D.S. Selishchev, D.V. Kozlov, UV-LED photocatalytic oxidation of carbon monoxide over TiO_2 supported with noble metal nanoparticles, Chem. Eng. J. 314 (2017) 600–611.
[35] Y. Chen, Y. Wang, W. Li, Q. Yang, Q. Hou, L. Wei, L. Liu, F. Huang, M. Ju, Enhancement of photocatalytic performance with the use of noble-metal-decorated TiO_2 nanocrystals as highly active catalysts for aerobic oxidation under visible-light irradiation, Appl. Catal. B Environ. 210 (2017) 352–367.
[36] A. Takai, P.V. Kamat, Capture, store and discharge. Shuttling photogenerated electrons across TiO_2-silver interface, ACS Nano 5 (2011) 7369–7376.
[37] L. Diamandescu, M. Feder, F. Vasiliu, L. Tanase, C.M. Teodorescu, T. Popescu, I. Dumitrescu, A. Sobetkii, Hydrothermal route to (Fe, N) codoped titania photocatalysts with increased visible light activity, Ind. Textila. 68 (2017) 303–308.
[38] S.A. Ansari, M.M. Khan, M.O. Ansari, M.H. Cho, Nitrogen-doped titanium dioxide (N-doped TiO_2) for visible light photocatalysis, New J. Chem. 40 (2016) 3000–3009.
[39] D. Wang, J. Li, G. Zhou, W. Wang, X. Zhang, X. Pan, Low temperature hydrothermal synthesis of visible-light-activated I-doped TiO_2 for improved dye degradation, J. Nanosci. Nanotechnol. 16 (2016) 5676–5682.
[40] C. Zheng, D. Li, J. Wan, X. Yu, Z. Xing, One-step synthesis of Ce–N–C–S-codoped TiO_2 catalyst and its enhanced visible light photocatalytic activity, J. Nanosci. Nanotechnol. 16 (2016) 12573–12581.
[41] L. Matějová, K. Kočí, I. Troppová, M. Šihor, M. Edelmannová, J. Lang, L. Čapek, Z. Matěj, P. Kuśtrowski, L. Obalová, TiO_2 and nitrogen doped TiO_2 prepared by different methods; on the (micro)structure and photocatalytic activity in CO_2 reduction and N_2O decomposition, J. Nanosci. Nanotechnol. 18 (2018) 688–698.
[42] P. Singla, O.P. Pandey, K. Singh, Study of photocatalytic degradation of environmentally harmful phthalate esters using Ni-doped TiO_2 nanoparticles, Int. J. Environ. Sci. Technol. (Tehran) 13 (2016) 849–856.
[43] D. Dvoranová, V. Brezová, M. Mazúr, M.A. Malati, Investigations of metal-doped titanium dioxide photocatalysts, Appl. Catal. B Environ. 37 (2002) 91–105.
[44] M.M. Momeni, Y. Ghayeb, Z. Ghonchegi, Photocatalytic properties of Cr–TiO_2 nanocomposite photoelectrodes produced by electrochemical anodisation of titanium, Surf. Eng. 32 (2016) 520–525.
[45] M.-Y. Xie, K.-Y. Su, X.-Y. Peng, R.-J. Wu, M. Chavali, W.-C. Chang, Hydrogen production by photocatalytic water-splitting on Pt-doped TiO_2–ZnO under visible light, J. Taiwan Inst. Chem. Eng. 70 (2017) 161–167.
[46] W. Shu-Xin, M. Zhi, Q. Yong-Ning, Q. Xiao-Zhou, L. Zhen-Cheng, Photocatalytic redox activity of doped nanocrystalline TiO_2, Acta Phys.-Chim. Sin. 20 (2004) 138–143.
[47] T. Ali, P. Tripathi, A. Azam, W. Raza, A.S. Ahmed, A. Ahmed, M. Muneer, Photocatalytic performance of Fe-doped TiO_2 nanoparticles under visible-light irradiation, Mater. Res. Express 4 (2017) 15022–15033.
[48] M. Freitag, J. Teuscher, Y. Saygili, X. Zhang, F. Giordano, P. Liska, J. Hua, S.M. Zakeeruddin, J.E. Moser, M. Grätzel, A. Hagfeldt, Dye-sensitized solar cells for efficient power generation under ambient lighting, Nat. Photonics 11 (2017) 372–378.
[49] A.K. Jana, Solar cells based on dyes, J. Photochem. Photobiol. A: Chem. 132 (2000) 1–17.
[50] M. Shakeel Ahmad, A.K. Pandey, N. Abd Rahim, Advancements in the development of TiO_2 photoanodes and its fabrication methods for dye sensitized solar cell (DSSC) applications. A review, Renew. Sustain. Energy Rev. 77 (2017) 89–108.
[51] R.D. Shannon, J.A. Pask, Kinetics of the anatase-rutile transformation, J. Am. Ceram. Soc. 48 (1965) 391–398.
[52] G. Balasubramanian, D.D. Dionysiou, M.T. Suidan, I. Baudin, J.-M. Laîné, Evaluating the activities of immobilized TiO_2 powder films for the photocatalytic degradation of organic contaminants in water, Appl. Catal. B Environ. 47 (2004) 73–84.
[53] Y. Yu, W. Wen, X.Y. Qian, J. Bin Liu, J.M. Wu, UV and visible light photocatalytic activity of Au/TiO_2 nanoforests with Anatase/Rutile phase junctions and controlled Au locations, Sci. Rep. 7 (2017) 1–13.
[54] S. Daneshvar e Asl, S.K. Sadrnezhaad, Two-phase rutile/anatase TiO_2 nanobranched nanorod arrays for photoelectrochemical applications, J. Adv. Mater. Eng. 37 (2018).
[55] H. Zhu, J. Tao, T. Wang, J. Deng, Growth of branched rutile TiO_2 nanorod arrays on F-doped tin oxide substrate, Appl. Surf. Sci. 257 (2011) 10494–10498.
[56] S. Linic, P. Christopher, D.B. Ingram, Plasmonic-metal nanostructures for efficient conversion of solar to chemical energy, Nat. Mater. 10 (2011) 911–921.
[57] X. Zhou, G. Liu, J. Yu, W. Fan, Surface plasmon resonance-mediated photocatalysis by noble metal-based, J. Mater. Chem. 22 (2012) 21337–21354.
[58] Y. Tian, T. Tatsuma, Plasmon-induced photoelectrochemistry at metal nanoparticles supported on nanoporous TiO_2, Chem. Commun. (2004) 1810–1811.
[59] R. Jiang, H. Chen, L. Shao, Q. Li, J. Wang, Unraveling the evolution and nature of the plasmons in (Au Core)-(Ag Shell) nanorods, Adv. Mater. 24 (2012) 1–8.
[60] A. Romanyuk, P. Oelhafen, Formation and electronic structure of TiO_2-Ag interface, Sol. Energy Mater. Sol. Cells 91 (2007) 1051–1054.
[61] Y. Yin, Z.-Y. Li, Z. Zhong, B. Gates, Y. Xia, S. Venkateswaran, Synthesis and characterization of stable aqueous dispersions of silver nanoparticles through the Tollens process, J. Mater. Chem. 12 (2002) 522–527.

[62] I. Tanabe, T. Tatsuma, Plasmonic manipulation of color and morphology of single silver nanospheres, Nano Lett. 12 (2012) 5418–5421.
[63] X. Dong, X. Ji, H. Wu, L. Zhao, J. Li, W. Yang, Shape control of silver nanoparticles by stepwise citrate reduction, J. Phys. Chem. C. 113 (2009) 6573–6576.
[64] Z. Jin, F. Wang, J. Wang, J.C. Yu, J. Wang, Metal nanocrystal-embedded hollow mesoporous TiO_2 and ZrO_2 microspheres prepared with polystyrene nanospheres as carriers and templates, Adv. Funct. Mater. 23 (2013) 2137–2144.
[65] S. Daneshvar e Asl, A. Eslami Saed, S.K. Sadrnezhaad, Hierarchical rutile/anatase TiO_2 nanorod/nanoflower thin film: Synthesis and characterizations, Mater. Sci. Semicond. Process. 93 (2019) 252–259.
[66] P. Yuan, R. Ma, N. Gao, M. Garai, Q.-H. Xu, Plasmon coupling enhanced two-photon photoluminescence of Au@Ag core-shell nanoparticles and applications in nuclease assay, Nanoscale. 13 (2017) 297–305.
[67] N.R. Jana, L. Gearheart, C.J. Murphy, Seeding growth for size control of 5-40 nm diameter gold nanoparticles, Langmuir 17 (2001) 6782–6786.
[68] T.K. Sau, C.J. Murphy, Seeded high yield synthesis of short Au nanorods in aqueous solution, Langmuir 20 (2004) 6414–6420.
[69] A. Gole, C.J. Murphy, Seed-mediated synthesis of gold nanorods: Role of the size and nature of the seed, Chem. Mater. 16 (2004) 3633–3640.
[70] N.R. Jana, L. Gearheart, C.J. Murphy, Wet chemical synthesis of high aspect ratio cylindrical gold nanorods, J. Phys. Chem. B 105 (2001) 4065–4067.
[71] J.M. Wu, T.W. Zhang, Y.W. Zeng, S. Hayakawa, K. Tsuru, A. Osaka, Large-scale preparation of ordered titania nanorods with enhanced photocatalytic activity, Langmuir 21 (2005) 6995–7002.
[72] J.M. Wu, T.W. Zhang, Photodegradation of rhodamine B in water assisted by titania films prepared through a novel procedure, J. Photochem. Photobiol. A: Chem. 162 (2004) 171–177.
[73] J. Wang, T. Zhang, D. Wang, R. Pan, Q. Wang, H. Xia, Improved morphology and photovoltaic performance in TiO_2 nanorod arrays based dye sensitized solar cells by using a seed layer, J. Alloys. Compd. 551 (2013) 82–87.
[74] M. Abd-Lefdil, R. Diaz, H. Bihri, M.A. Aouaj, F. Rueda, Preparation and characterization of sprayed FTO thin films, Eur. Phys. J. Appl. Phys. 28 (2007) 217–219.
[75] D.O. Scanlon, C.W. Dunnill, J. Buckeridge, S.A. Shevlin, A.J. Logsdail, S.M. Woodley, C.R.A. Catlow, M.J. Powell, R.G. Palgrave, I.P. Parkin, G.W. Watson, T.W. Keal, P. Sherwood, A. Walsh, A.A. Sokol, Band alignment of rutile and anatase TiO_2, Nat. Mater. 12 (2013) 798–801.
[76] H. Tang, K. Prasad, R. Sanjinès, P.E. Schmid, F. Lévy, Electrical and optical properties of TiO_2 anatase thin films, J. Appl. Phys. 75 (1994) 2042–2047.
[77] J.C. Yu, J. Yu, W. Ho, Z. Jiang, L. Zhang, Effects of F- doping on the photocatalytic activity and microstructures of nanocrystalline TiO_2 powders, Chem. Mater. 14 (2002) 3808–3816.
[78] W.F. Zhang, M.S. Zhang, Z. Yin, Q. Chen, Photoluminescence in anatase titanium dioxide nanocrystals, Appl. Phys. B Lasers Opt. 70 (2000) 261–265.
[79] J. Yu, L. Yue, S. Liu, B. Huang, X. Zhang, Hydrothermal preparation and photocatalytic activity of mesoporous Au-TiO_2 nanocomposite microspheres, J. Colloid Interface Sci. 334 (2009) 58–64.
[80] J. Yu, J. Ran, Facile preparation and enhanced photocatalytic H_2-production activity of $Cu(OH)_2$ cluster modified TiO_2, Energy Environ. Sci. 4 (2011) 1364–1371.
[81] I.S. Cho, Z. Chen, A.J. Forman, D.R. Kim, P.M. Rao, T.F. Jaramillo, X. Zheng, Branched TiO_2 nanorods for photoelectrochemical hydrogen production, Nano Lett. 11 (2011) 4978–4984.
[82] A. Nakaruk, D. Ragazzon, C.C. Sorrell, Anatase-rutile transformation through high-temperature annealing of titania films produced by ultrasonic spray pyrolysis, Thin Solid Films 518 (2010) 3735–3742.
[83] D.Y. Lee, J.T. Kim, J.H. Park, Y.H. Kim, I.K. Lee, M.H. Lee, B.Y. Kim, Effect of Er doping on optical band gap energy of TiO_2 thin films prepared by spin coating, Curr. Appl. Phys. 13 (2013) 1301–1305.
[84] A. Nakaruk, C.Y. Lin, D.S. Perera, C.C. Sorrell, Effect of annealing temperature on titania thin films prepared by spin coating, J. Solgel Sci. Technol. 55 (2010) 328–334.
[85] D. Mardare, M. Tasca, M. Delibas, G.I. Rusu, On the structural properties and optical transmittance of TiO_2r.f. sputtered thin films, Appl. Surf. Sci. 156 (2000) 200–206.
[86] R. López, R. Gómez, Band-gap energy estimation from diffuse reflectance measurements on sol-gel and commercial TiO_2: a comparative study, J. Solgel Sci. Technol. 61 (2012) 1–7.
[87] D. Tsukamoto, Y. Shiraishi, Y. Sugano, S. Ichikawa, S. Tanaka, T. Hirai, Gold nanoparticles located at the interface of anatase/rutile TiO_2 particles as active plasmonic photocatalysts for aerobic oxidation, J. Am. Chem. Soc. 134 (2012) 6309–6315.